Journal of Pharmaceutical Analysis 12 (2022) 232–242

Contents lists available at ScienceDirect

Journal of Pharmaceutical Analysis

journal homepage: www.elsevier.com/locate/jpa

Original article

Development of a novel multi-functional integrated bioconjugate effectively targeting K-Ras mutant pancreatic cancer

Yang-Yang Wang [a, b], Liang Li [b], Xiu-Jun Liu [b], Qing-Fang Miao [b, **], Yi Li [b], Meng-Ran Zhang [b], Yong-Su Zhen [b, *]

[a] Department of Pediatric Oncology, Tianjin Medical University Cancer Institute and Hospital, Tianjin, 300060, China
[b] NHC Key Laboratory of Biotechnology of Antibiotics, Department of Oncology, Institute of Medicinal Biotechnology, Chinese Academy of Medical Sciences & Peking Union Medical College, Beijing, 100050, China

ARTICLE INFO

Article history:
Received 12 October 2020
Received in revised form
17 June 2021
Accepted 2 July 2021
Available online 3 July 2021

Keywords:
Pancreatic cancer
Folate receptor
Multi-functional
Macropinocytosis-enhanced
Bioconjugate
K-Ras
PEGylation

ABSTRACT

Folate receptor (FR) overexpression occurs in a variety of cancers, including pancreatic cancer. In addition, enhanced macropinocytosis exists in K-Ras mutant pancreatic cancer. Furthermore, the occurrence of intensive desmoplasia causes a hypoxic microenvironment in pancreatic cancer. In this study, a novel FR-directed, macropinocytosis-enhanced, and highly cytotoxic bioconjugate folate (F)-human serum albumin (HSA)-apoprotein of lidamycin (LDP)-active enediyne (AE) derived from lidamycin was designed and prepared. F-HSA-LDP-AE consisted of four moieties: F, HSA, LDP, and AE. F-HSA-LDP presented high binding efficiency with the FR and pancreatic cancer cells. Its uptake in wild-type cells was more extensive than in K-Ras mutant-type cells. By in vivo optical imaging, F-HSA-LDP displayed prominent tumor-specific biodistribution in pancreatic cancer xenograft-bearing mice, showing clear and lasting tumor localization for 360 h. In the MTT assay, F-HSA-LDP-AE demonstrated potent cytotoxicity in three types of pancreatic cancer cell lines. It also induced apoptosis and caused G2/M cell cycle arrest. F-HSA-LDP-AE markedly suppressed the tumor growth of AsPc-1 pancreatic cancer xenografts in athymic mice. At well-tolerated doses of 0.5 and 1 mg/kg, (i.v., twice), the inhibition rates were 91.2% and 94.8%, respectively ($P<0.01$). The results of this study indicate that the F-HSA-LDP multi-functional bioconjugate might be effective for treating K-Ras mutant pancreatic cancer.

1. Introduction

Pancreatic ductal adenocarcinoma (PDAC) is fatal, and its mortality is closely related to morbidity. Most patients with pancreatic cancer are asymptomatic until the disease progresses to an advanced stage [1,2]. Pancreatic cancer has four driver genes: K-Ras, tumor protein p53, SMAD family member 4, and cyclin-dependent kinase inhibitor 2A (CDKN2A). K-Ras and CDKN2A mutations are usually associated with early pancreatic cancer. Over ninety percent of PDAC contains mutations in K-Ras oncogene, particularly in K-Ras^{G12D} [3]. During the past three decades, all protein drugs that directly target K-Ras have failed because K-Ras lacks structural targets to bind small molecules or drugs. Therefore, K-Ras is widely considered to be "undruggable" [4]. Due to the complexity of the K-Ras signaling pathway and the resistance of K-Ras-mutant tumors to clinical drugs, there are currently no effective drugs or methods for treating K-Ras-mutant tumors. Consequently, several studies have focused on indirect strategies [5,6]. In addition, previous studies have suggested that oncogenic K-Ras alters extracellular fluid uptake and utilization and that the K-Ras oncogene can promote upregulation of micropinocytosis [7,8]. Macropinocytosis is a kind of endocytosis in which cells take extracellular fluid and solutes from the extracellular environment into endocytic vesicles called macrosomes. This mechanism is different from autophagy [9]. There is evidence that PDAC cells expressing oncogenic K-Ras use macropinocytosis to transport extracellular fluid into cells to maintain tumor growth [10,11]. As previously reported, tumor cells with mutant K-Ras display elevated levels of macropinocytosis, employing human serum albumin (HSA) as the main source of nutrients [12]. Therefore, it is

Peer review under responsibility of Xi'an Jiaotong University.
* Corresponding author.
** Corresponding author.
E-mail addresses: miaoqf@imb.pumc.edu.cn (Q.-F. Miao), zhenys@imb.pumc.edu.cn (Y.-S. Zhen).

https://doi.org/10.1016/j.jpha.2021.07.001

feasible to use HSA as a macrophage-mediated drug delivery vehicle in K-Ras targeted therapy.

Folate receptors (FRs) are a class of membrane receptors. FRα, FRβ, FRγ, and FRδ (FR family members) have been found to bind with folate closely [13]. The α-isoform of FR is selectively overexpressed in some tumors although it exhibits minimal expression in normal tissues [14]. There are three main routes for folate uptake. First, intestinal folate absorption occurs through the proton-coupled folate transporter at an acidic pH. Second, the uptake of folate by reduced folate carrier α, widely expressed in a wide range of tissues, is achieved at physiological pH. Due to the hydrophilic anionic nature of folates, the last route involves endocytosis through FRs [15,16]. In addition, most FRs are only expressed on the top surface of normal cells to prevent the exposure of FRs to the folate supplied by the blood. In tumorigenesis, the vasculature becomes chaotic and disorganized, leading to a weak link between endothelial cells. In addition, the changes in the entire structure result in FRs that do not have a polarized cell location and are then randomly distributed on the entire cell surface, making FR more accessible to FR-directed drug conjugates in circulation [17,18]. In several clinical trials of FR-positive cancers, many FR-targeted antibody-drug conjugates and small molecule drugs have been used, indicating that FR-targeted therapy can bring promising clinical benefits.

Interstitial desmoplasia, the hallmark of pancreatic cancer, provides a unique microenvironment that affects pancreatic tumor behavior, causing dense fibrosis around cancer cells. Therefore, hypoxia helps tumor growth and metastasis, a common microenvironmental feature in tumor masses, particularly in PDAC [19]. Cancer cells in a hypoxic state are generally more resistant to cytotoxic agents. Therefore, it is important to find an agent highly potent against cancer cells in the hypoxic microenvironment. It is reported that lidamycin (LDM), also known as C-1027, is more cytotoxic in a hypoxic than a normoxic environment. It may be associated with many solid tumor (including PDAC) cells in a hypoxic microenvironment [20]. Thus, LDM appears to be an attractive agent to serve as the "warhead" moiety of targeting drugs against tumors with a hypoxic microenvironment. LDM, a member of the enediyne antibiotic family derived from *Streptomyces*, has strong cytotoxicity to various cancer cells. It is composed of active enediyne (AE) derived from LDM chromophore and LDM apoprotein (LDP) and can dissociate and recombine under certain conditions in vitro. The AE chromophore of LDM is responsible for its strong cytotoxicity, and the hydrophobic pocket formed by LDP can protect AE [21–23]. According to the structural characteristics of LDM, our group has previously constructed various LDM-derived fusion proteins through genetic engineering. The protein is composed of different antibody fragments, which are directed against specific antigens in tumors. Albumin-based LDM has shown high therapeutic efficacy for lung cancer xenografts in nude mice [24,25]. LDM can be used as a highly effective "warhead" molecule for constructing various targeted anti-cancer therapies.

Based on the macropinocytosis-enhanced and FR-overexpressed behavior of K-Ras mutant pancreatic cancer cells, we designed and generated a novel multi-functional recombinant protein conjugate in three major steps: DNA recombination, chemical conjugation, and molecular reconstitution. The FR-directed and macropinocytosis-enhanced recombinant protein conjugate folate (F)-HSA-LDP-AE consists of four moieties: F, HSA, LDP, and AE, where F and HSA are connected by polyethylene glycol (PEG). This recombinant protein conjugate exerts effective cytotoxicity in cultured cancer cells, shows specific tumor localization and long-lasting accumulation, and is effective for K-Ras mutant PDAC xenotransplantation in athymic mouse.

2. Methods

2.1. Cell culture

The PDAC cell lines BxPc-3, AsPc-1, and MIA PaCa-2 were obtained from the American Type Culture Collection. All cells were cultured at 37 °C under 5% CO_2. AsPC-1 and BxPC-3 cells were cultured in RPMI 1640 medium (Hyclone, Logan, UT, USA) supplemented with 10% fetal bovine serum (Gibco, Grand Island, NY, USA) and 1% penicillin-streptomycin solution. MIA PaCa-2 cells were cultured in DMEM medium (Hyclone, Logan, UT, USA) supplemented with 10% fetal bovine serum and 1% penicillin-streptomycin solution.

2.2. Preparation and purification of F-HSA-LDP and F-HSA-LDP-AE

2.2.1. Expression and purification of the recombination protein HSA-LDP

Pichia pastoris strains GS115 expressing the recombinant HSA-LDP protein were preserved in our laboratory [25]. The culture conditions were previously published by our research group. HSA-LDP was purified with nickel ion affinity chromatography using His Trap FF columns (GE Healthcare, Chicago, IL, USA).

2.2.2. Folate conjugation

Aldehyde functional F-PEG (molecular weight (MW) = 10 kDa) was purchased from Ponsai Biotechnology (Shanghai, China). A 5 mg/mL HSA-LDP in 20 mM sodium phosphate buffer containing 25 mM sodium cyanoborohydride (pH 6.0) was used and stirred at 4 °C for 12 h to perform the coupling reaction. F-PEG was added at a PEG/protein molar ratio of 5:1. At 25 °C, F-HSA-LDP was separated from unbound F-PEG and HSA-LDP by anion exchange chromatography on a diethylaminoethyl Sepharose FF column. The reaction mixture was loaded on the DEAE column and washed with 20 mM Tris buffer (pH 8.0) until no protein was eluted. Thereafter, five column volumes were used to elute the column with a linear gradient of 0.1–0.5 M NaCl in 20 mM Tris buffer. Elution was detected at 280 nm. The fractions containing F-HSA-LDP were collected by ÄKTA™ chromatography system (GE Healthcare, Boston, MA, USA) and desalted by PD-10 desalting column. The product was analyzed by size exclusion chromatography (Agilent 1200; Agilent Technologies, Savage, MD, USA) on a TSK G3000SWXL gel filtration column (Tosoh, Tokyo, Japan). Thereafter, 20 μL of the sample was loaded onto the column with an isocratic mobile phase of 10 mM phosphate buffered saline (PBS, pH 7.2), 1 mL/min flow rate, and a UV absorbance of 280 nm.

2.2.3. Molecular reconstitution

In the 25% acetonitrile mobile phase containing 0.025% trifluorolactic acid, the AE of LDM was separated on a C_4 column. F-HSA-LDP was added to produce a 1:5 M ratio of conjugate/AE. The reaction was performed in the dark at 4 °C with stirring for 12 h. Therafter, a membrane with 30 kDa cut off value (Millipore, Burlington, MA, USA) was used to remove free AE by ultrafiltration. The absorbance of the solution was detected at 340 nm.

2.3. In vitro binding affinity assay

2.3.1. Enzyme-linked immunoassay

The binding affinity of LDP, HSA-LDP, and F-HSA-LDP to FR proteins and pancreatic cancer cells was determined using ELISA according to the manufacturer's protocol (Cusabio, Wuhan, China).

2.3.2. Flow cytometry analysis

The binding affinity of different concentrations of fluorescein isothiocyanate (FITC)-labeled HSA-LDP and F-HSA-LDP to PDAC cells was also analyzed by flow cytometry. A total of 5×10^4 cells were incubated with various concentrations of FITC-labeled HSA-LDP and F-HSA-LDP at 4 °C for 2 h. After washing three times with PBS, the cells were analyzed by BD FACSCalibur (BD Biosciences, San Jose, CA, USA).

2.4. In vitro internalization assay

Furthermore, 5×10^4 cells/well were seeded on 8-well glass chamber slides (Millicell, Billerica, MA, USA). After culturing for 24 h, the cells were washed three times with PBS and combined with 5 μM FITC-labeled recombinant protein and tetramethylrhodamine (TMR)-dextran (MW = 70,000; Invitrogen, Carlsbad, CA, USA) or 50 μM ethyl-isopropyl amiloride (EIPA) (Sigma, St. Louis, MO, USA), and was placed at 37 °C for 2 h. Thereafter, the cells were washed three times with PBS and fixed in 4% formaldehyde at 25 °C for 1 h. After staining the nuclei with 4',6-diamidino-2-phenylindole (DAPI), the cellular uptake of F-HSA-LDP was confirmed with a fluorescence microscope.

2.5. In vivo optical imaging system

Female athymic BALB/c (*nu/nu*) mice (18–22 g) were purchased from SPF Biotechnology (Beijing, China). AsPc-1 tumor-bearing mice were injected intravenously with 20 mg/kg of LDP, HSA-LDP, and F-HSA-LDP, respectively, and labeled with DyLight 680 microscale antibody labeling kit (Thermo Fisher Scientific, Waltham, MA, USA). Thereafter, a small animal in vivo imaging system (Xenogen, Alameda, CA, USA) was used to image the mice with excitation and emission wavelengths of 675 nm and 720 nm, respectively.

2.6. Cell viability assay

The cells were seeded in a 96-well plate (5×10^3 cells/well) and incubated with concentrations of recombinant protein. Thereafter, the medium was poured out, 5 mg/mL of methyl tetrazolium (MTT) was added into 20 μL of PBS and incubated for another 4 h. Thereafter, the medium was removed, and 150 μL of dimethyl sulfoxide was added per well. The absorbance was quantified at 570 nm (Multiskan MK3; Thermo LabSystems, Waltham, MA, USA).

2.7. Cell cycle arrest and apoptosis assays

The Annexin V-FITC/propidium iodide (PI) cell apoptosis kit (Solarbio, Beijing, China) was used to assess cell apoptosis. The cells were innoculated into a 6-well tissue culture plate (2×10^5 cells/well). After processing various concentrations of the recombinant protein to be tested and conjugated for 24 h, the cells were collected, washed with PBS three times, and then resuspended in 500 μL of binding buffer. Thereafter, 5 μL of Annexin V-FITC and 5 μL of PI were added into the buffer and incubated in the dark at 25 °C for 15 min. For cell cycle arrest assay, cells were collected and washed in PBS, then fixed in 70% ethanol, incubated with RNase (50 μg/mL) and 50 μg/mL PI solution, and protected from light at 25 °C for 30 min. BD FACSCalibur flow cytometer (BD Biosciences, San Jose, CA, USA) was used to measure cell cycle and apoptosis analysis.

2.8. In vivo efficacy studies

Female athymic BALB/c (*nu/nu*) mice (18–22 g) were purchased from SPF Biotechnology (Beijing, China). AsPc-1 cells (6×10^6) suspended in 200 μL of sterile saline were inoculated s.c. in the right armpit of all nude mice. When the tumor size was over 100 mm^3, mice were divided into groups (n=8) and treated with different doses of F-HSA-LDP-AE, F-HSA-LDP, HSA-LDP-AE, LDM, and nab-paclitaxel. All of the tested agents were injected i.v. into the tail vein with 200 μL of sterile saline. One week after the first treatment, all nude mice were injected with secondary doses. Tumor sizes were measured every 2 days, and tumor volume was determined by the formula: length × width^2/2. On day 28, tumors were removed from the mice and weighed, and the inhibition rate was calculated according to the following formula: $[1-(V_{tf}-V_{ti})/(V_{cf}-V_{ci})] \times 100\%$, where V_{tf} and V_{ti} represent the final and initial tumor volumes of the treatment group, and V_{cf} and V_{ci} represent the final and initial tumor volumes of the control group, respectively. At the end of the experiment, the mice were euthanized. Various organs and tumors were harvested and fixed in 10% formalin for histopathological examination (HE staining). Ethics Committee approval was obtained from the Institutional Ethics Committee of Peking Union Medical College (IMB-20180820D7 and IMB-20180701D7) to the commencement of the study.

2.9. Statistical analysis

All data were statistically analyzed using GraphPad Prism 5. A t-test (two-tailed) was performed, and $P<0.05$ was considered statistically significant. The data are expressed as mean ± standard deviation.

3. Results

3.1. Preparation and characterization of the recombinant protein conjugate

We designed and generated the recombinant protein conjugate in three major steps: DNA recombination, chemical conjugation, and molecular reconstitution. Fig. 1A shows the preparation procedure and structures of HSA-LDP, F-HSA-LDP, and F-HSA-LDP-AE. First, our group previously developed the fusion protein HSA-LDP by genetic engineering [25]. Secondly, through reductive alkylation between the aldehyde group of 10 kDa F-PEG and the free N-terminal α-amino group of HSA-LDP, the FR-directed protein conjugate F-HSA-LDP was obtained. Then F-PEG propionaldehyde was selectively bound to the α-amino group of the N-terminal amino acid residue of HSA-LDP. The preparation process was as follows. The coupled reaction was performed with stirring at 4 °C for 12 h using 5 mg/mL HSA-LDP in 20 mM sodium phosphate buffer containing 25 mM sodium cyanoborohydride (pH 6.0). The F-PEG was added at a 5:1 M ratio of PEG/protein. Thereafter, F-HSA-LDP was separated from the unconjugated F-PEG and HSA-LDP by anion exchange chromatography on a DEAE Sepharose FF column at 25 °C. Third, the cytotoxic enediyne molecule AE derived from LDM was assembled with F-HSA-LDP to obtain F-HSA-LDP-AE. As shown in Fig. 1B, SDS-PAGE analysis confirmed the presence of HSA-LDP protein purified from the HSA-LDP fermentation broth supernatant. Fig. 1C shows the SEC-HPLC analysis of F-HSA-LDP at 280 nm, and Fig. 1D shows the reversed-phase HPLC analysis of enediyne-integrated F-HSA-LDP-AE at 340 nm using a C_4 column. The peaks before the first 5 min were the system peaks in the reverse-phase HPLC, which were the superimposed peaks of trifluoroacetic acid (TFA) and acetonitrile and the inverted peaks due to the cavitation effect of the additive TFA. The peak at 9.9 min was the characteristic absorption peak of F-HSA-LDP-AE. Fig. 1 shows the preparation and characterization of the recombinant protein conjugate F-HSA-LDP and F-HSA-LDP-AE.

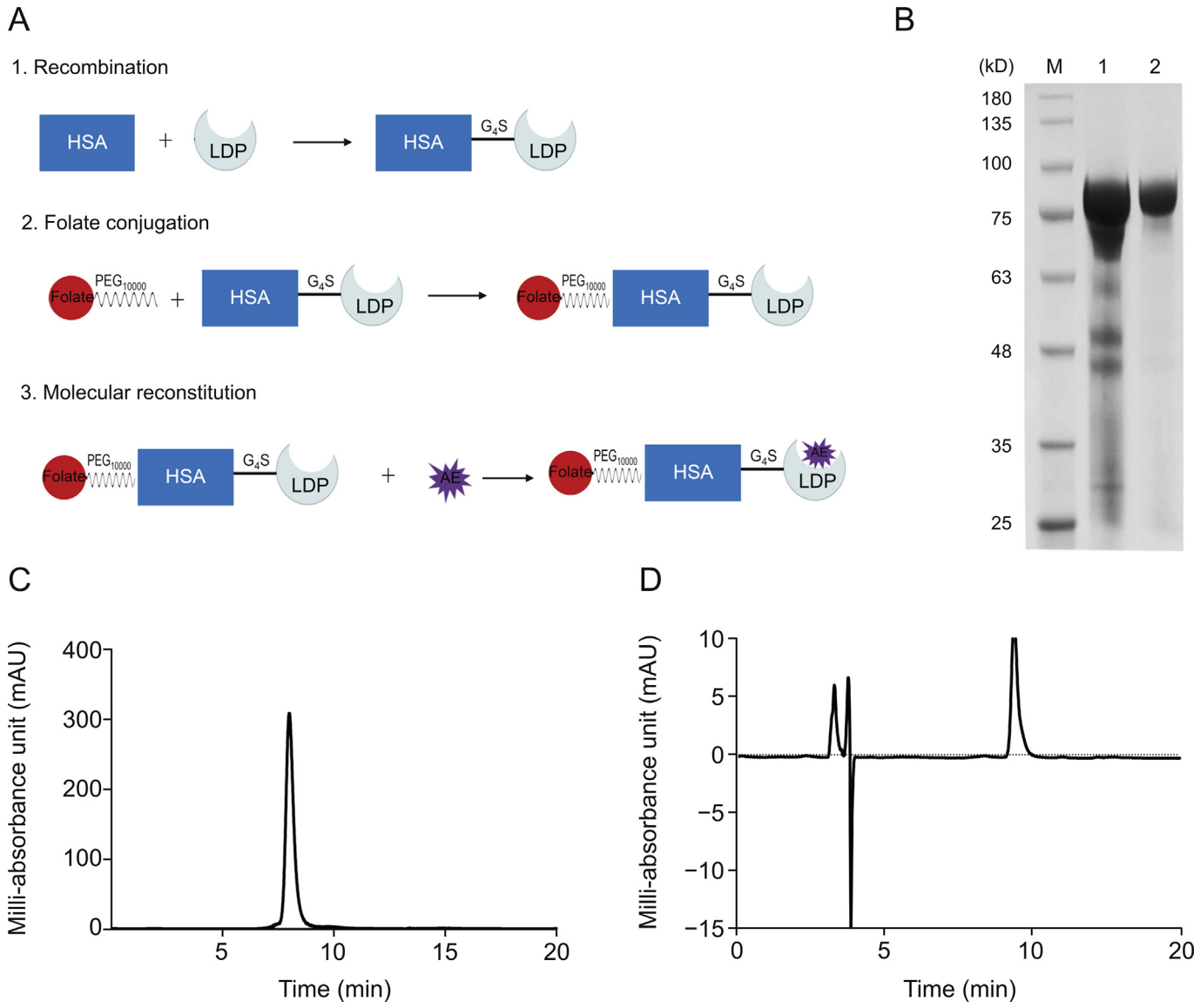

Fig. 1. Characterization of HSA-LDP, F-HSA-LDP, and F-HSA-LDP-AE. (A) Schema of the constitution and preparation process of F-HSA-LDP-AE. (B) SDS-PAGE analysis of HSA-LDP (M: marker; 1: supernatant of HSA-LDP fermentation broth; 2: purified HSA-LDP recombinant protein). (C) SEC-HPLC analysis of F-HSA-LDP at 280 nm. (D) Reverse-phase HPLC analysis of enediyne-integrated F-HSA-LDP-AE using a C_4 column at 340 nm. The peak at 9.9 min is the characteristic absorption peak of F-HSA-LDP-AE. LDM: lidamycin; LDP: the apoprotein of LDM; AE: the active enediyne derived from LDM; HSA: human serum albumin; F-HSA-LDP: recombinant protein conjugate of folate (F) and HSA-LDP; F-HSA-LDP-AE: F-HSA-LDP reconstituted with AE.

3.2. Binding activity of the recombinant protein conjugate in vitro

ELISA and flow cytometry were conducted to analyze the binding activities of LDP, HSA-LDP, and F-HSA-LDP to FR and pancreatic tumor cell lines. The recombinant protein conjugate F-HSA-LDP presented high binding efficiency, and HSA-LDP presented weak binding activity with FR, whereas minimal binding efficiency of the LDP was observed, as shown in Fig. 2A. Furthermore, F-HSA-LDP displayed high binding capacity with the three tested pancreatic cancer cell lines, whereas only weak binding capacity with the cells was detected in HSA-LDP. Thereafter, we labeled different concentrations of LDP, HSA-LDP, and F-HSA-LDP with FITC, co-incubated them with pancreatic cancer cells, and detected the fluorescence intensity by flow cytometry. As shown in Fig. 2B, the affinity of FITC-labeled LDP, HSA-LDP and F-HSA-LDP to pancreatic cancer cell lines tested by flow cytometry was similar to ELISA. These results illustrate that F-HSA-LDP had better affinity to pancreatic cancer cells compared to LDP and HSA-LDP.

3.3. Enhanced macropinocytosis of the recombinant protein conjugate in PDAC cells

K-Ras mutations have been reported to be present in more than 90% of pancreatic cancers, whereas K-Ras-mutated tumor cells are accompanied by significant macropinocytosis and can take up more proteins and nutrients [7]. Therefore, we selected BxPc-3 cells with wild-type K-Ras and AsPc-1 cells with mutant K-Ras as the subjects to observe their uptake of F-HSA-LDP. Green fluorescence represents FITC-labeled F-HSA-LDP protein, blue fluorescence represents DAPI-stained nucleus, and red fluorescence represents TMR-dextran. After incubation with FITC-labeled recombinant protein conjugate F-HSA-LDP (5 μM) at 37 °C for 30 min, different levels of cellular uptake were observed in BxPc-3 and AsPc-1 pancreatic cells. As shown in Fig. 3A, F-HSA-LDP showed effective uptake related to its binding activity. K-Ras mutant AsPc-1 cells positively affected recombinant protein conjugate F-HSA-LDP ($P<0.01$, Fig. 3B), compared with K-Ras wild-type BxPc-3 cells. The uptake of

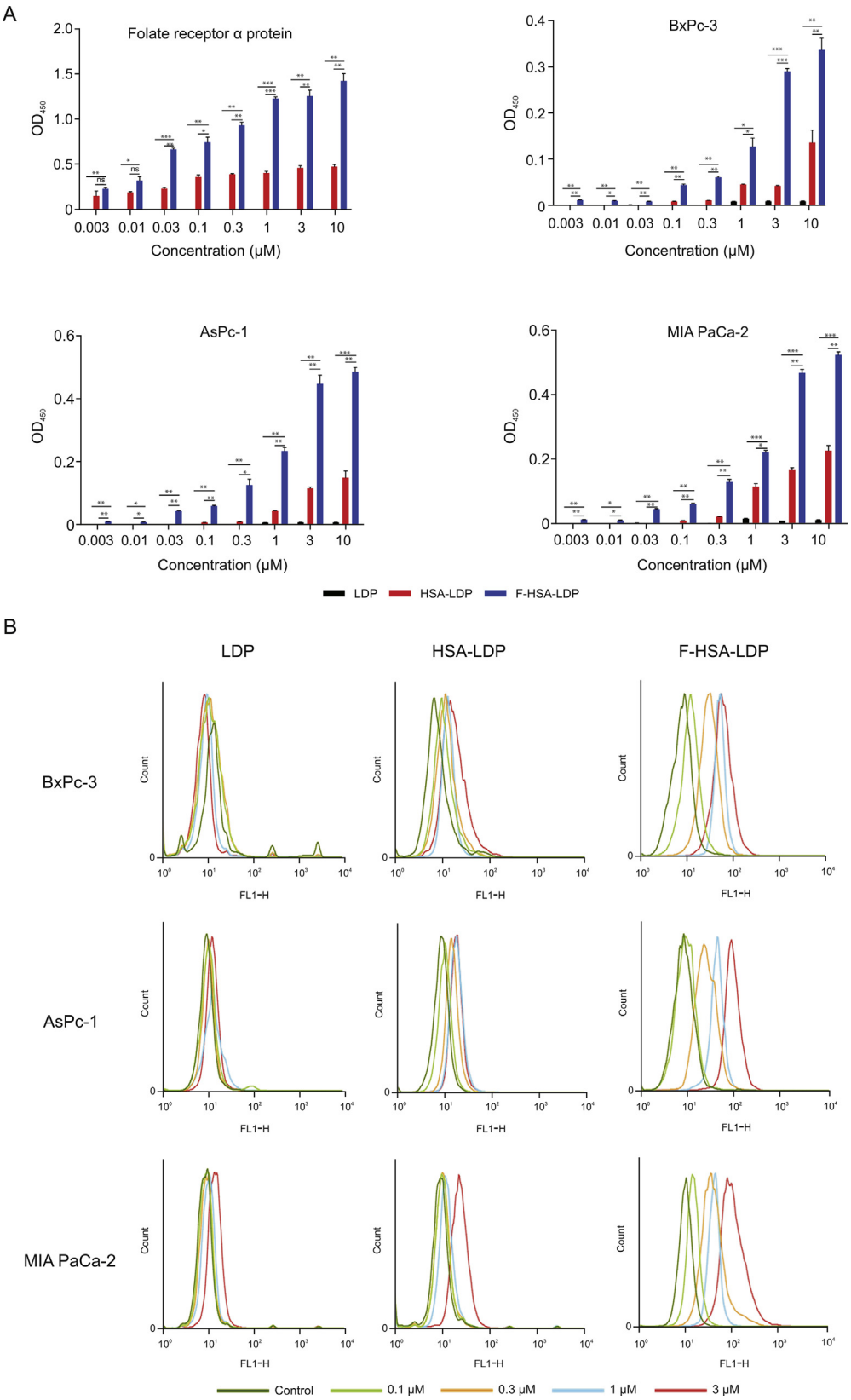

Fig. 2. Binding activity of the recombinant protein and conjugate in vitro. (A) ELISA of the binding activities of LDP, HSA-LDP, and F-HSA-LDP to FR protein and pancreatic cancer cells, $^{*}P<0.05$, $^{**}P<0.01$, $^{***}P<0.001$. (B) Binding affinity of FITC-labeled LDP, HSA-LDP, and F-HSA-LDP to pancreatic cancer cells, as detected by flow cytometry analysis. FR: folate receptor; FITC: fluorescein isothiocyanate.

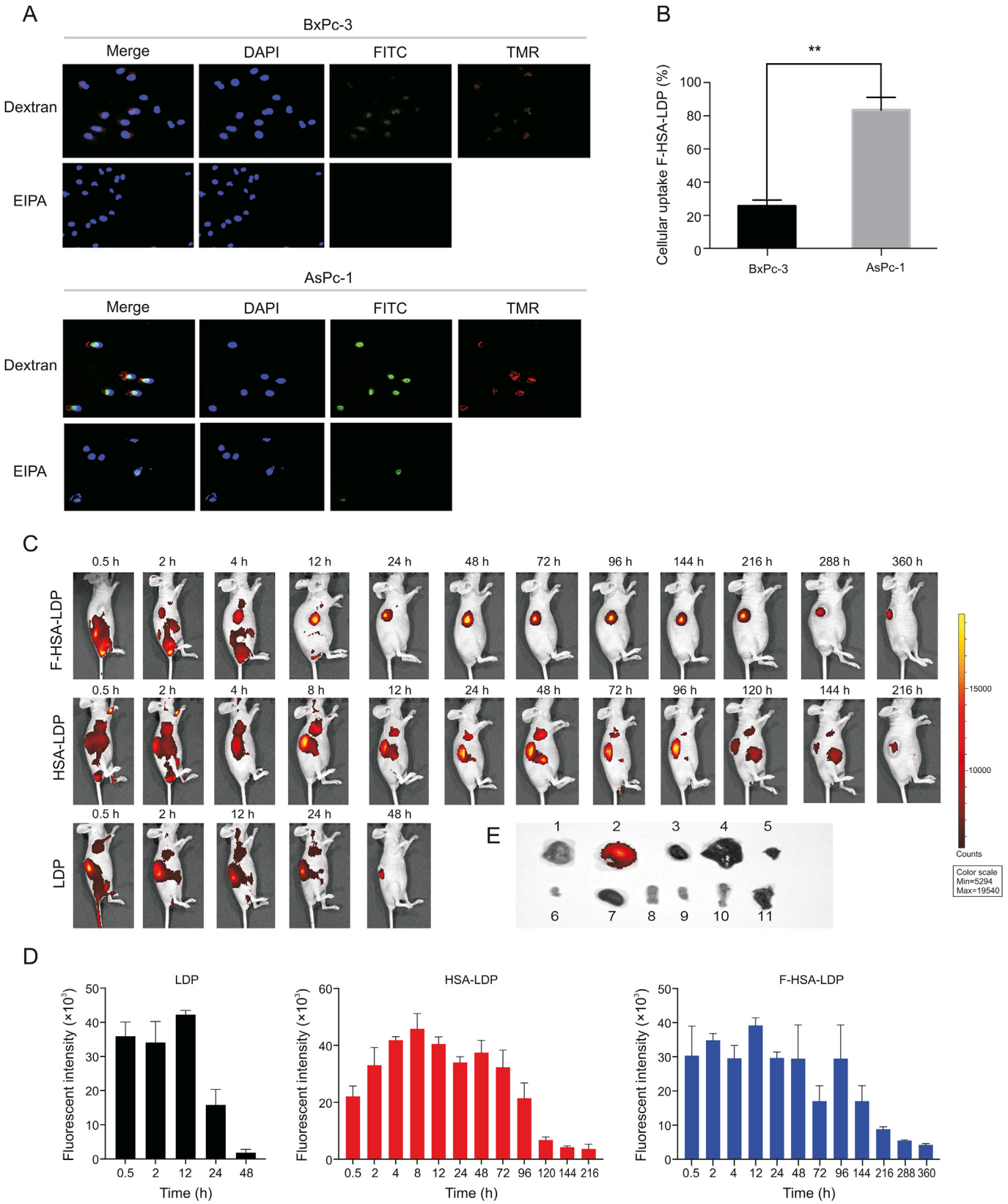

Fig. 3. Binding and uptake of the recombinant protein conjugate in vitro and the imaging in vivo. (A) Uptake of F-HSA-LDP in BxPc-3 and AsPc-1 cells determined by fluorescence microscopy. The merged image was detected with FITC-labeled recombinant protein conjugate (green), DAPI staining (blue) and TMR-dextran (red) (immunofluorescence ×200). (B) The percentage of cellular uptake F-HSA-LDP in BxPc-3 and AsPc-1 cells, $^{**}P<0.01$. (C) Fluorescent images of the AsPc-1 tumor xenograft in athymic mice were obtained at different time intervals after tail vein injection of DyLight 680-labeled recombinant protein and conjugate at 20 mg/kg. (D) Fluorescent intensity of DyLight 680-labeled LDP, HSA-LDP, and F-HSA-LDP in vivo. (E) After in vivo observation, the fresh tumor and various organs were removed for imaging (1–11: Day 1–Day 11). Day 1 and Day 2, tumors taken from the HSA-LDP and F-HSA-LDP injected mice, respectively. Day 3 to Day 11 in various organs from F-HSA-LDP-injected mice; the images represent the heart, liver, spleen, pancreas, kidney, small and large intestine, femur bone marrow, and lung, respectively. All images were acquired from the in vivo imaging system-200. DAPI: 4',6-diamidino-2-phenylindole; TMR: tetramethylrhodamine ; EIPA: ethyl-isopropyl amiloride.

LDP was greater. Cell internalization was mediated through giant pinocytosis. This was further confirmed by incubation with the specific inhibitors of mega cytosis, EIPA, and TMR-dextran (a marker of mega cytosis). In vitro cell experiments revealed that F-HSA-LDP could better bind to the surface of pancreatic cancer cells than HSA-LDP and LDP and internalize into tumor cells through K-Ras-mediated macropinocytosis enhancement.

3.4. In vivo fluorescence imaging of F-HSA-LDP, HSA-LDP, and LDP

To further compare the targeting of the three proteins in vivo, we also used an optical molecular imaging system to observe the fluorescence signals of DyLight 680-labeled F-HSA-LDP, HSA-LDP, and LDP in pancreatic cancer AsPc-1 xenograft nude mice to determine the tissue distribution and tumor target accumulation ability. The DyLight 680-labeled LDP control protein was administered at a dose of 20 mg/kg. Thereafter, the fluorescence decreased rapidly within 48 h (Figs. 3C and D). Simultaneously, the fluorescent signals of HSA-LDP and F-HSA-LDP were initially visible at the tumor site within 48 h, and the tumor localization image of F-HSA-LDP was clearly maintained for 360 h. DyLight 680-labeled HSA-LDP was clearly distributed in the liver and other organs, whereas most of DyLight 680-labeled F-HSA-LDP precisely targeted the tumor site, thereby reducing the toxicity to non-tumor tissues and organs. Fluorescent signals can still be detected in tumors of mice injected with F-HSA-LDP, except in tumors of HSA-LDP group and other tested organs, including heart, liver, spleen, pancreas, kidney, large intestine, small intestine, bone marrow and lung (Fig. 3E). As previously mentioned, F-HSA-LDP shows highly specific biodistribution and long-term tumor localization and accumulation in the AsPc-1 pancreatic cancer model.

Table 1
IC_{50} values for LDM, HSA-LDP-AE and F-HSA-LDP-AE against various pancreatic cancer cell lines.

Cell lines	IC_{50} (nM)		
	LDM	HSA-LDP-AE	F-HSA-LDP-AE
BxPc-3	$(1.21 \pm 0.13) \times 10^{-1}$	$(1.51 \pm 0.21) \times 10^{-1}$	$(8.12 \pm 1.78) \times 10^{-2}$
AsPc-1	$(8.56 \pm 4.56) \times 10^{-3}$	$(8.49 \pm 1.20) \times 10^{-2}$	$(5.55 \pm 2.72) \times 10^{-3}$
MIA PaCa-2	$(9.31 \pm 3.65) \times 10^{-2}$	$(9.26 \pm 0.11) \times 10^{-2}$	$(3.54 \pm 0.47) \times 10^{-2}$

IC_{50} values were calculated using the SPSS software. Data are presented as mean ± standard deviation from three independent experiments. LDM: lidamycin; LDP: apoprotein of LDM; AE: active enediyne derived from LDM; HSA: human serum albumin; F-HSA-LDP: recombinant protein conjugate of folate and HSA-LDP; F-HSA-LDP-AE: F-HSA-LDP reconstituted with AE.

3.5. In vitro cytotoxicity of the recombinant protein conjugate

The FR-directed recombinant protein conjugate F-HSA-LDP was further integrated with extremely cytotoxic AE to produce F-HSA-LDP-AE, and the cytotoxicity was measured using the MTT assay. A comparative test was also conducted on LDM. AsPc-1 and MIA PaCa-2 cells are K-Ras mutants, and BxPc-3 cells are K-Ras wild type. As shown in Fig. 4, F-HSA-LDP-AE exerted strong cytotoxicity in three tested PDAC AsPc-1, BxPc-3, and MIA PaCa-2 cells, with IC_{50} values of 0.006–0.08 nM (Table 1). Among these three cell lines,

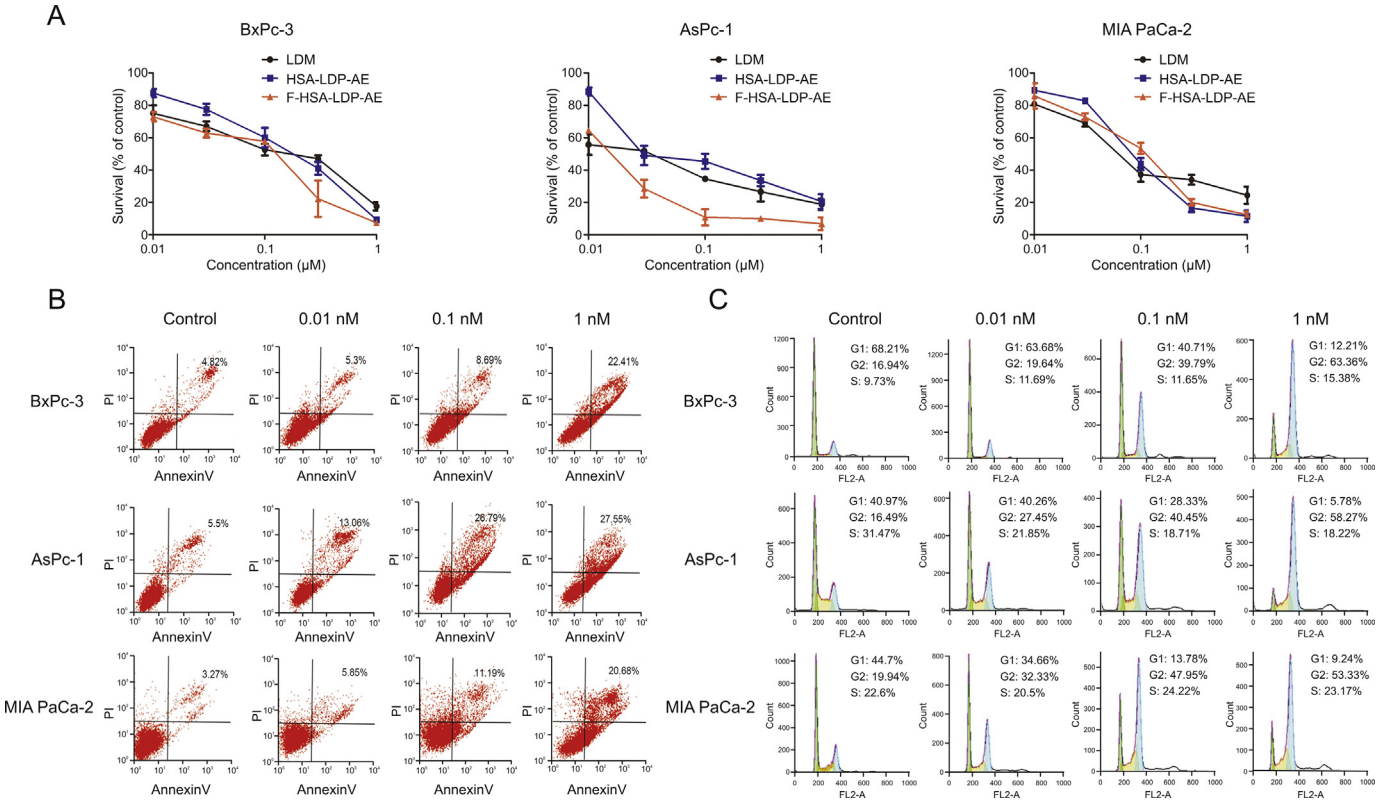

Fig. 4. Bioactivity analysis of the recombinant protein conjugate. (A) The cytotoxicity of LDM, HSA-LDP-AE, and F-HSA-LDP-AE to AsPc-1, BxPc-3 and MIA PaCa-2 cells, as determined by the methyl tetrazolium assay. (B) Induction of apoptosis in three pancreatic cancer cell lines was observed by flow cytometry. All cells were treated with various concentrations of F-HSA-LDP-AE for 24 h. (C) Cell cycle arrest analysis in three pancreatic cancer cell lines was detected by flow cytometry. Cells were treated with various concentrations of F-HSA-LDP-AE for 24 h.

AsPc-1 cells were more sensitive to F-HSA-LDP-AE with an IC_{50} value of 0.006 nM. In addition, the cytotoxicity of F-HSA-LDP-AE was slightly higher than that of HSA-LDP-AE and LDM (Fig. 4A). Pancreatic cancer cells BxPc-3, AsPc-1, MIA PaCa-2 were treated with different concentrations of F-HSA-LDP-AE drugs for 24 h and detected by flow cytometry. Apoptosis analysis showed that when treated with F-HSA-LDP-AE, the ratio of AsPc-1, BxPc-3, and MIA PaCa-2 cell apoptosis increased in a concentration-dependent manner (Fig. 4B). F-HSA-LDP-AE led to G2/M cell cycle arrest at 0.1 nM (Fig. 4C).

3.6. In vivo therapeutic efficacy

In vivo efficacy was tested in a nude mouse model of AsPc-1 xenograft. Mice carrying AsPc-1 xenografts were divided into eight groups and treated intravenously with LDM, F-HSA-LDP, F-HSA-LDP-AE, HSA-LDP-AE, or nab-paclitaxel, respectively, for twice with one week apart. According to previous studies [25], the doses of HSA-LDP-AE and nab-paclitaxel were 0.8 and 200 mg/kg, respectively, and the doses of F-HSA-LDP-AE were 0.25, 0.5 and 1 mg/kg according to the pre-experimental results (Fig. S1). Control mice received no treatment. The mice tolerated all the procedures of the treatment groups well and did not significantly lose weight (Fig. 5A). As shown in Figs. 5B and C, F-HSA-LDP-AE significantly inhibited the growth of pancreatic cancer xenografts. At doses of 0.5 and 1 mg/kg, F-HSA-LDP-AE inhibited tumor growth by 91.2% and 94.8%, respectively. The efficacy of F-HSA-LDP-AE was much stronger than that of HSA-LDP-AE, LDM, and nab-paclitaxel. In addition, the inhibition rate of F-HSA-LDP-AE at 1 mg/kg was statistically significantly different from that of LDM at the tolerated dose of 0.1 mg/kg (inhibition rate of 64.5%) and nab-paclitaxel at the dose of 200 mg/kg (inhibition rate of 55%). F-HSA-LDP showed a moderate inhibitory effect on tumor growth at 20 mg/kg (inhibition rate of 44%). As shown in Fig. 5D, immunohistochemical staining was compared to calculate the mitotic index (Ki-67 expression) of the treatment group and the control group of tumor-bearing mice to evaluate the F-HSA-LDP and F-HSA-LDP-AE pair proliferation of AsPc-1 tumor cells. Strong immunohistochemical staining against the cell proliferation index Ki-67 was observed in the tumor tissues of the control group, whereas moderate levels were found in F-HSA-LDP (20 mg/kg) and F-HSA-LDP-AE (1 mg/kg) weak staining group (P<0.001, Fig. 5E). The results showed that F-HSA-LDP-AE treatment had a significant anti-proliferative effect on tumor cells in vivo. In addition, the heart, lung, liver, stomach, small intestine, kidney, spleen, and bone marrow of mice treated with 1 mg/kg F-HSA-LDP-AE showed no toxicological or pathological changes (Fig. 6), indicating that the high-efficiency dose of the recombinant protein conjugate F-HSA-LDP-AE did not cause pathological changes in various tissues and organs.

4. Discussion

The failed trials of farnesyl transferase inhibitors and the unsatisfactory results of the downstream inhibition of mitogen-activated protein kinases/extracellular signal-regulated kinase demonstrate the unprecedented challenge of effectively targeting K-Ras [5]. In addition, K-Ras mediates cellular and metabolic transformations during tumorigenesis, and tumor progression is driven by gene mutations [6]. Compared with K-Ras wild-type cells, K-Ras mutant tumor cells show higher glucose uptake and a higher glutamine dependence on biosynthetic reactions [9,26]. In addition, compared to the K-Ras wild-type counterpart, the K-Ras mutant non-small cell lung cancer cell line is more dependent on the folate metabolism pathway. In addition, the expression of

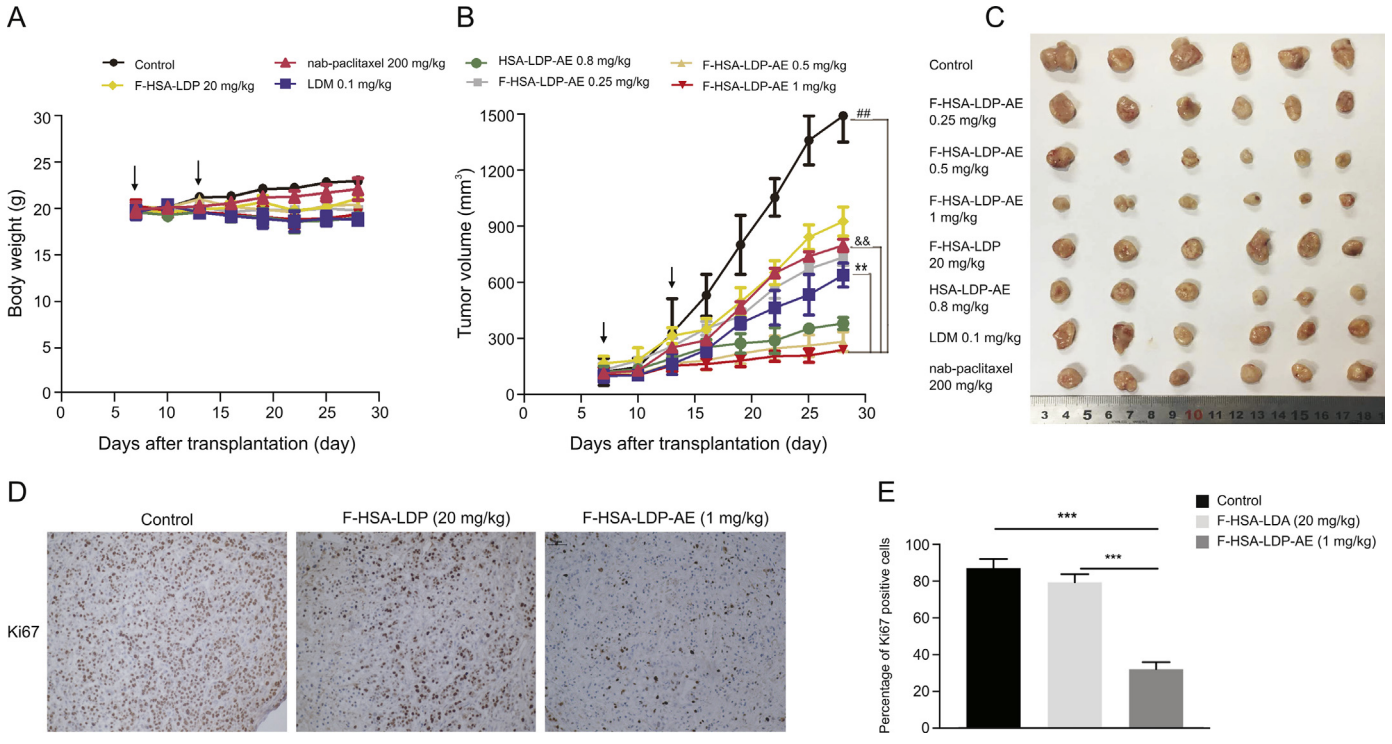

Fig. 5. In vivo therapeutic efficacy. (A) Body weight changes curves of the AsPc-1 xenograft-bearing mice. (B) Tumor growth curves in AsPc-1 xenograft-bearing athymic mice treated with FR-directed recombinant protein conjugate F-HSA-LDP-AE and other agents (n=8). $^{\#\#}P$<0.01 compared with the control group; $^{**}P$<0.01 compared with the LDM group (0.1 mg/kg); $^{\&\&}P$<0.01 compared with the nab-paclitaxel group (200 mg/kg). Arrows denote the days of injection. (C) Representative tumor tissue images from all groups of mice (n=8) after sacrifice at day 28. (D) Immunohistochemical staining for Ki67 in the control group, F-HSA-LDP group (20 mg/kg), and F-HSA-LDP-AE group (1 mg/kg) (immunohistochemical staining ×200). (E) The percentage of Ki67 positive cells, $^{***}P$<0.001.

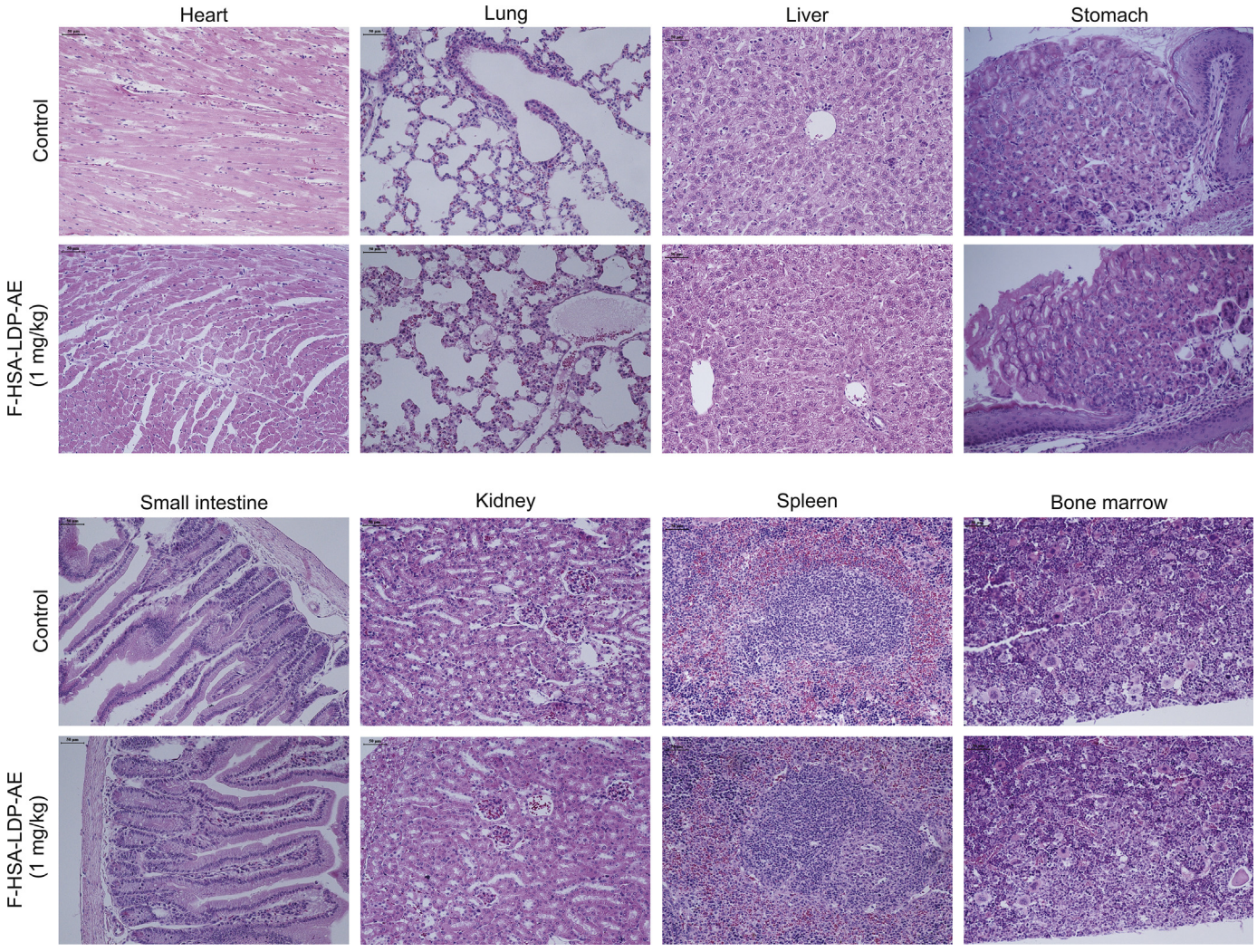

Fig. 6. HE staining of various organs from AsPc-1 xenograft-bearing mice treated with F-HSA-LDP-AE (1 mg/kg) and the control group. The histopathological observations from various organs of the control and F-HSA-LDP-AE (1 mg/kg) group from AsPc-1 xenograft-bearing mice. No toxicopathological changes were found in heart, lung, liver, stomach, small intestine, kidney, spleen, or bone marrow (HE ×200).

genes related to purine biosynthesis and folate metabolism has increased. The altered regulation of folate metabolism in K-Ras mutant cancer cells may explain the higher antifolate activity [27,28]. Some evidence supports the fact that activating K-Ras can promote cellular protein uptake. In particular, K-Ras mutant cells strongly rely on enhanced macropinocytosis to transport extracellular proteins into cells to maintain their proliferation and growth [10,29]. Therefore, albumin integration can develop targeted anticancer drugs against K-Ras mutant PDAC [30–32]. This study confirmed that the uptake of the recombinant protein conjugate F-HSA-LDP in K-Ras mutant pancreatic cancer cells was increased, and the large amount of entry was blocked by the specific inhibitor EIPA, indicating that the intensive uptake was mediated by giant pinocytosis.

The preferred chemotherapy regimen for patients with PDAC is FOLFIRINOX (5-fluorouracil, calcium folinate, irinotecan, oxaliplatin) combined with gemcitabine and nab-paclitaxel [33], suggesting that folate may be a highly relevant molecule in the treatment and indicating that FR might be used as a molecular target. In contrast to the restricted FR expression found in normal tissues, many cancers, including pancreatic cancer, do express one or more FRs. FRα has been found in pancreatic cancer, breast cancer, ovarian cancer, head and neck cancer, lung cancer, bladder cancer, kidney cancer, and colon cancer. Approximately 40% of human cancers overexpress FR [34,35]. A previous study using immunohistochemical analysis showed that in 22 (16%), 73 (52%) and 45 (32%) specimens of 140 PDAC patients, FRα expression intensity was low, moderate, and high, respectively [36]. From the database of Encyclopedia of Cancer Cell Lines, at the mRNA level, FRα is highly expressed in pancreatic cancer after breast cancer according to the incidence rate [35]. Therefore, folate binding is a potential method to target FR-positive tumor tissues for personalized treatment. For the absorption of folate, in contrast to most normal cells that rely on reduced folate carriers, most pancreatic cancer cells overexpress one or more high-affinity FRs on their surface, which may reflect their increased demand for folate to support rapid cell growth [37]. Cancer cell proliferation is more dependent on folate than normal somatic cells; therefore, folate antagonists that interfere with this biochemical pathway have been widely used in cancer treatment since the 1940s, becoming the first chemotherapy drug [38]. However, the clinical use of folate antagonists is not selective for FRα. Previous studies have found that the entry of folate into cells is receptor-mediated endocytosis. Therefore, folate has been used as a guide molecule for targeting FR [34]. Therefore, coupling folate and

its analogues with "warhead" drugs can specifically bind to FR and selectively enrich in FR-rich tissues, that is, various tumors. This study designed and produced a multi-functional FR-directed recombinant protein conjugate F-HSA-LDP and its enediyne-integrated conjugate F-HSA-LDP-AE. The results showed that the purified F-HSA-LDP exhibits specific binding affinity to FR protein in various pancreatic cancer cells and shows its outstanding tumor-specific localization and long-lasting accumulation, and F-HSA-LDP-AE has a very high therapeutic effect.

The AE is a highly cytotoxic DNA damage agent produced by microbial secondary metabolism with a common structural motif. The biological activity of AE is driven by its interaction with target DNA. Cycloaromatization of AE core produces a nascent benzodiradical that induces the capture of hydrogen atoms from the deoxyribose backbone near DNA. Furthermore, the formed deoxyribose-centered radical can react with molecular oxygen to generate single-strand breaks, double-strand breaks (DSBs), or interstrand crosslinks (ICLs). These DNA lesions are responsible for the cytotoxicity of AE. LDM exhibits threefold enhanced cytotoxicity against hypoxic cells. This function is attributed to AE-derived from LDM to produce oxygen-independent ICLs in addition to conventional DSBs [39]. Although DSBs and ICLs operate under normoxic conditions, ICL production is significantly enhanced under hypoxic conditions that inhibit DSBs, thus providing a strategy for treating refractory tumors in a hypoxic microenvironment.

According to previous studies, PEGylation can increase the size of protein and extend its half-life by reducing the glomerular filtration rate in the kidney. Therefore, the biological distribution of the protein is changed [40,41]. The product of site-specific modification is a homogeneous product with fewer isomers, better activity, and significantly reduced immunogenicity [42]. The N-terminal PEGylation of HSA-LDP protein shows site-specific covalent binding and utilizes the difference in pKa value between the N-terminal α-amino group and ε-amino group of lysine residues. HSA has 58 lysine residues at most, and the pKa value of its N-terminal α-amino group is approximately 8.0, which is much lower than that of the lysine residue ε-amino group (pKa 10.8). Due to the low pKa, PEG-propionaldehyde has strong selectivity to the N-terminal α-amino group under acidic conditions [43–46]. In this study, the PEGylation of protein drugs was shown to be effective.

5. Conclusions

The newly developed FR-directed, macropinocytosis-enhanced and highly cytotoxic multi-functional agent might be effective for K-Ras mutant pancreatic cancer therapy. First, F-HSA-LDP showed specific binding to FR and the tested cancer cells. Second, it was extensively taken up by the target cells through macropinocytosis. Third, it displayed specific biodistribution in the pancreatic cancer xenograft-bearing athymic mice with a clear and lasting image of tumor localization. Fourth, the enediyne-integrated conjugate F-HSA-LDP-AE exerted potent cytotoxicity in target cancer cells. Finally, it showed high therapeutic efficacy to a K-Ras mutant PDAC xenograft. Therefore, these results suggest that our FR-directed, macropinocytosis-enhanced, and highly cytotoxic integrative strategy is feasible for generating drugs that effectively target K-Ras mutant pancreatic cancer.

CRediT author statement

Yang-Yang Wang: Conceptualization, Methodology, Software, Validation, Investigation, Data curation, Writing - Original draft preparation, Reviewing and Editing, Visualization; **Liang Li:** Methodology; **Xiu-Jun Liu:** Methodology; **Qing-Fang Miao:** Conceptualization, Methodology, Formal analysis, Resources, Writing - Reviewing and Editing, Supervision; **Yi Li:** Investigation; **Meng-Ran Zhang:** Investigation; **Yong-Su Zhen:** Conceptualization, Methodology, Formal analysis, Resources, Writing - Reviewing and Editing, Supervision.

Declaration of competing interest

The authors declare that there are no conflicts of interest.

Acknowledgments

This work was supported by grants from CAMS Innovation Fund for Medical Sciences (Grant No.: 2021-I2M-1-026), Scientific Research Project of Tianjin Education Commission (Grant No.: 2020KJ140), and Tianjin Health Research Project (Grant No.: KJ20017). The authors are grateful for all the participants in this study.

Appendix A. Supplementary data

Supplementary data to this article can be found online at https://doi.org/10.1016/j.jpha.2021.07.001.

References

[1] T. Kamisawa, L.D. Wood, T. Itoi, et al., Pancreatic cancer, Lancet 388 (2016) 73–85.
[2] H. Thomas, Pancreatic cancer: infiltrating macrophages support liver metastasis, Nat. Rev. Gastroenterol. Hepatol. 13 (2016), 313.
[3] E. Costello, W. Greenhalf, J.P. Neoptolemos, New biomarkers and targets in pancreatic cancer and their application to treatment, Nat. Rev. Gastroenterol. Hepatol. 9 (2012) 435–444.
[4] J.B. Fleming, G.L. Shen, S.E. Holloway, et al., Molecular consequences of silencing mutant K-ras in pancreatic cancer cells: justification for K-ras-directed therapy, Mol. Cancer Res. 3 (2005) 413–423.
[5] H. Jung, S. Park, G.R. Gunassekaran, et al., A peptide probe enables photoacoustic-guided imaging and drug delivery to lung tumors in K-ras(LA2) mutant mice, Cancer Res. 79 (2019) 4271–4282.
[6] E. Rozengurt, G. Eibl, Central role of Yes-associated protein and WW-domain-containing transcriptional co-activator with PDZ-binding motif in pancreatic cancer development, World J. Gastroenterol. 25 (2019) 1797–1816.
[7] K.L. Bryant, J.D. Mancias, A.C. Kimmelman, et al., KRAS: feeding pancreatic cancer proliferation, Trends Biochem. Sci. 39 (2014) 91–100.
[8] X. Wang, W. Sheng, Y. Wang, et al., A macropinocytosis-intensifying albumin domain-based scFv antibody and its conjugate directed against K-ras mutant pancreatic cancer, Mol. Pharm. 15 (2018) 2403–2412.
[9] P.M. Thu, Z.G. Zheng, Y.P. Zhou, et al., Phellodendrine chloride suppresses proliferation of KRAS mutated pancreatic cancer cells through inhibition of nutrients uptake via macropinocytosis, Eur. J. Pharmacol. 850 (2019) 23–34.
[10] C. Commisso, S.M. Davidson, R.G. Soydaner-Azeloglu, et al., Macropinocytosis of protein is an amino acid supply route in Ras-transformed cells, Nature 497 (2013) 633–637.
[11] H. Ying, A.C. Kimmelman, C.A. Lyssiotis, et al., Oncogenic Kras maintains pancreatic tumors through regulation of anabolic glucose metabolism, Cell 149 (2012) 656–670.
[12] D. Gaglio, C.M. Metallo, P.A. Gameiro, et al., Oncogenic K-Ras decouples glucose and glutamine metabolism to support cancer cell growth, Mol. Syst. Biol. 7 (2011), 523.
[13] H. Shi, J. Guo, C. Li, et al., A current review of folate receptor alpha as a potential tumor target in non-small-cell lung cancer, Drug Des. Devel. Ther. 9 (2015) 4989–4996.
[14] H. Kurahara, S. Takao, T. Kuwahata, et al., Clinical significance of folate receptor β–expressing tumor-associated macrophages in pancreatic cancer, Ann. Surg Oncol. 19 (2012) 2264–2271.
[15] R.C. Lynn, M. Poussin, A. Kalota, et al., Targeting of folate receptor β on acute myeloid leukemia blasts with chimeric antigen receptor-expressing T cells, Blood 125 (2015) 3466–3476.
[16] Y.G. Assaraf, C.P. Leamon, J.A. Reddy, The folate receptor as a rational therapeutic target for personalized cancer treatment, Drug Resist. Updat. 17 (2014) 89–95.
[17] M. Fernández, F. Javaid, V. Chudasama, Advances in targeting the folate receptor in the treatment/imaging of cancers, Chem. Sci. 9 (2017) 790–810.
[18] S. Chittiboyina, Z. Chen, E.G. Chiorean, et al., The role of the folate pathway in pancreatic cancer risk, PLoS One 13 (2018), e0193298.
[19] J. Wang, J. Shen, K. Zhao, et al., STIM1 overexpression in hypoxia microenvironment contributes to pancreatic carcinoma progression, Cancer Biol. Med. 16 (2019) 100–108.

[20] T.A. Beerman, L.S. Gawron, S. Shin, et al., C-1027, a radiomimetic enediyne anticancer drug, preferentially targets hypoxic cells, Cancer Res. 69 (2009) 593–598.
[21] X.F. Guo, X.F. Zhu, Y. Shang, et al., A bispecific enediyne-energized fusion protein containing ligand-based and antibody-based oligopeptides against epidermal growth factor receptor and human epidermal growth factor receptor 2 shows potent antitumor activity, Clin. Cancer Res. 16 (2010) 2085–2094.
[22] L. Li, B. Shang, L. Hu, et al., Site-specific PEGylation of lidamycin and its antitumor activity, Acta Pharm. Sin. B 5 (2015) 264–269.
[23] R. Wang, L. Li, S. Zhang, et al., A novel enediyne-integrated antibody-drug conjugate shows promising antitumor efficacy against CD30(+) lymphomas, Mol. Oncol. 12 (2018) 339–355.
[24] Y.H. Huang, B.Y. Shang, Y.S. Zhen, Antitumor efficacy of lidamycin on hepatoma and active moiety of its molecule, World J. Gastroenterol. 11 (2005) 3980–3984.
[25] L. Li, L. Hu, C.Y. Zhao, et al., The recombinant and reconstituted novel albumin-lidamycin conjugate shows lasting tumor imaging and intensively enhanced therapeutic efficacy, Bioconjug. Chem. 29 (2018) 3104–3112.
[26] J. Yun, C. Rago, I. Cheong, et al., Glucose deprivation contributes to the development of KRAS pathway mutations in tumor cells, Science 325 (2009) 1555–1559.
[27] D.M. Moran, P.B. Trusk, K. Pry, et al., KRAS mutation status is associated with enhanced dependency on folate metabolism pathways in non-small cell lung cancer cells, Mol. Cancer Ther. 13 (2014) 1611–1624.
[28] E.S. Schernhammer, E. Giovannuccci, C.S. Fuchs, et al., A prospective study of dietary folate and vitamin B and colon cancer according to microsatellite instability and KRAS mutational status, Cancer Epidemiol. Biomarker Prev. 17 (2008) 2895–2898.
[29] N. Santana-Codina, A.A. Roeth, Y. Zhang, et al., Oncogenic KRAS supports pancreatic cancer through regulation of nucleotide synthesis, Nat. Commun. 9 (2018), 4945.
[30] Y. Du, B.Y. Shang, W.J. Sheng, et al., A recombinantly tailored β-defensin that displays intensive macropinocytosis-mediated uptake exerting potent efficacy against K-Ras mutant pancreatic cancer, Oncotarget 7 (2016) 58418–58434.
[31] H. Liu, M. Sun, Z. Liu, et al., KRAS-enhanced macropinocytosis and reduced FcRn-mediated recycling sensitize pancreatic cancer to albumin-conjugated drugs, J. Contr. Release 296 (2019) 40–53.
[32] F. Islami, J. Ferlay, J. Lortet-Tieulent, et al., International trends in anal cancer incidence rates, Int. J. Epidemiol. 46 (2017) 924–938.
[33] H. Chen, R. He, X. Shi, et al., Meta-analysis on resected pancreatic cancer: a comparison between adjuvant treatments and gemcitabine alone, BMC Cancer 18 (2018), 1034.
[34] L.C. Hartmann, G.L. Keeney, W.L. Lingle, et al., Folate receptor overexpression is associated with poor outcome in breast cancer, Int. J. Cancer 121 (2007) 938–942.
[35] S. Omote, K. Takata, T. Tanaka, et al., Overexpression of folate receptor alpha is an independent prognostic factor for outcomes of pancreatic cancer patients, Med. Mol. Morphol. 51 (2018) 237–243.
[36] D.H. Josephs, H.J. Bax, T. Dodev, et al., Anti-folate receptor-α IgE but not IgG recruits macrophages to attack tumors via TNFα/MCP-1 signaling, Cancer Res. 77 (2017) 1127–1141.
[37] Z. Liu, X. Jin, W. Pi, et al., Folic acid inhibits nasopharyngeal cancer cell proliferation and invasion via activation of FRα/ERK1/2/TSLC1 pathway, Biosci. Rep. 37 (2017), BSR20170772.
[38] K. Cheung-Ong, G. Giaever, C. Nislow, DNA-damaging agents in cancer chemotherapy: serendipity and chemical biology, Chem. Biol. 20 (2013) 648–659.
[39] A. Adhikari, B. Shen, C. Rader, Challenges and opportunities to develop enediyne natural products as payloads for antibody-drug conjugates, Antib. Ther. 4 (2021) 1–15.
[40] E. Fahrländer, S. Schelhaas, A.H. Jacobs, et al., PEGylated human serum albumin (HSA) nanoparticles: preparation, characterization and quantification of the PEGylation extent, Nanotechnology 26 (2015), 145103.
[41] T. Yin, H. Cai, J. Liu, et al., Biological evaluation of PEG modified nanosuspensions based on human serum albumin for tumor targeted delivery of paclitaxel, Eur. J. Pharm. Sci. 83 (2016) 79–87.
[42] P. Akbarzadehlaleh, M. Mirzaei, M. Mashahdi-Keshtiban, et al., PEGylated human serum albumin: review of PEGylation, purification and characterization methods, Adv. Pharmaceut. Bull. 6 (2016) 309–317.
[43] T. Zhao, Y.N. Cheng, H.N. Tan, et al., Site-specific chemical modification of human serum albumin with polyethylene glycol prolongs half-life and improves intravascular retention in mice, Biol. Pharm. Bull. 35 (2012) 280–288.
[44] J.K. Dozier, M.D. Distefano, Site-specific PEGylation of therapeutic proteins, Int. J. Mol. Sci. 16 (2015) 25831–25864.
[45] H. Kang, S. Rho, W.R. Stiles, et al., Size-dependent EPR effect of polymeric nanoparticles on tumor targeting, Adv. Healthc. Mater. 9 (2020), e1901223.
[46] Y. Yang, W. Zhu, L. Cheng, et al., Tumor microenvironment (TME)-activatable circular aptamer-PEG as an effective hierarchical-targeting molecular medicine for photodynamic therapy, Biomaterials 246 (2020), 119971.